Sensitive and Specific CRISPR-Cas12a Assisted Nanopore With RPA For Monkeypox Detection

Md. Ahasan Ahamed¹, Muhammad Asad Ullah Khalid¹, Ming Dong¹, Anthony J. Politza², Zhikun Zhang¹, Aneesh Kshirsagar¹, Tianyi Liu¹, and Weihua Guan^{1, 2,*}

¹ Department of Electrical Engineering, Pennsylvania State University, University Park 16802, USA

² Department of Biomedical Engineering, Pennsylvania State University, University Park 16802, USA

^{*} Correspondence should be addressed to wzg111@psu.edu

Abstract

Monkeypox virus (MPXV) poses a global health emergency, necessitating rapid, simple, and accurate detection to manage its spread effectively. The Clustered Regularly Interspaced Short Palindromic Repeats (CRISPR) technique has emerged as a promising next-generation molecular diagnostic approach. Here, we developed a highly sensitive and specific CRISPR-Cas12a assisted nanopore (SCAN) with isothermal recombinase polymerase amplification (RPA) for MPXV detection. The RPA-SCAN method offers a sensitivity unachievable with unamplified SCAN while also addressing the obstacles of PCR-SCAN for point-of-care applications. We demonstrated that size-counting of single molecules enables analysis of reaction-time dependent distribution of the cleaved reporter. Our MPXV-specific RPA assay achieved a limit of detection (LoD) of 19 copies in a 50 µL reaction system. By integrating 2 µL of RPA amplifications into a 20 μL CRISPR reaction, we attained an overall LoD of 16 copies/μL (26.56 aM) of MPXV at a 95% confidence level using the SCAN sensor. We also verified the specificity of RPA-SCAN in distinguishing MPXV from cowpox virus with 100% accuracy. These findings suggest that the isothermal RPA-SCAN device is well-suited for highly sensitive and specific Monkeypox detection. Given its electronic nature and miniaturization potential, the RPA-SCAN system paves the way for diagnosing a wide array of other infectious pathogens at the point of care.

Keywords

Monkeypox, RPA-SCAN, CRISPR-Cas12a, RPA-CRISPR, Nanopore.

1. Introduction

The Monkeypox Virus (MPXV) is a zoonotic disease of an escalating global health concern due to its epidemic potential and rapidly increasing incidence (Chadha et al., 2022; Di Giulio and Eckburg, 2004). The genetic diversity of MPXV is complex, involving multiple variants with varying degrees of virulence(Okyay, 2022). Particularly concerning is the strain first identified in Massachusetts, USA, on May 17, 2022, associated with a high fatality rate of around 10% (Americo et al., 2023). According to the World Health Organization (WHO) report, this virulent strain has infected 3,487 people in 45 states in the USA (Elsayed et al., 2022). Simultaneously, the Centers for Disease Control and Prevention (CDC) monitors a global outbreak with 15,510 confirmed cases in 72 countries, including 5 deaths, all linked primarily to the strain originally discovered in the USA during the 2022 Monkeypox outbreak (Sharma et al., 2022). Therefore, it is crucial to develop reliable, rapid, and readily accessible testing techniques to manage and control this disease's spread effectively.

The ongoing quest for optimal point-of-care testing (POCT) strategies has driven the development of advanced nucleic acid testing (NAT) platforms. The quantitative polymerase chain reaction (PCR) is currently the gold standard for NAT. Recent advancements in Clustered Regularly Interspaced Short Palindromic Repeats (CRISPR) based NAT detection methods have achieved high specificity (Chen et al., 2018; Kellner et al., 2019; Li et al., 2018). CRISPR-based methods utilize fluorescent, bioluminescent, or colorimetric reporters for readouts, often incorporating fluorescence resonance energy transfer (FRET) by labeling the reporter molecule with appropriate fluorophores (Ahamed et al., 2022). Pre-amplification processes such as PCR, loop-mediated isothermal amplification (LAMP) (Notomi et al., 2015), or recombinase polymerase amplification (RPA) (Lobato and O'Sullivan, 2018) are commonly used to enhance the sensitivity of the CRISPR methods (Nouri et al., 2021). However, these methods often rely on optical sensing, necessitating additional reporter molecules like fluorescence for detection. Integrating optical sensors into compact POCT devices poses challenges, including accurate alignment and incorporation of optical components (Dey et al., 2023). Recently, there has been a growing interest in electronic-based methodologies like electrochemical (Ali et al., 2021; Farooqi et al., 2021; Khalid et al., 2022), field-effect transistors (Sakata et al., 2005) and solid-state nanopore sensors (Kidan et al., 2018; Z. Wang et al., 2019), due to their potential for integration and miniaturization.

Previously, we developed the sensitive and specific CRISPR-Cas12a assisted nanopore (SCAN) sensor based on two approaches: with pre-amplification and without pre-amplification. We used pre-amplification to increase the sensor sensitivity (Nouri et al., 2021). In this pre-amplification technique, the SCAN system uses the PCR approach to amplify products, demonstrating its accuracy and specificity (Qin et al., 2019; Nouri et al., 2020). However, the demonstrated PCR pre-amplification is not amendable of POCT because it requires thermal modules such as temperature sensors and heaters for temperature cycling, often consuming high amounts of energy and power (Ahamed et al., 2020; Petralia and Conoci, 2017). With its isothermal properties, LAMP could be a suitable pre-amplification method for the SCAN, but its production of non-uniform size amplicons is unsuitable for SCAN applications. In this regard, RPA is a preferred pre-amplification method for SCAN due to low-temperature rapid isothermal amplification (Lau et al., 2016; Lillis et al., 2016). Integrating the RPA effectively with the SCAN sensor (RPA-SCAN) is critical to enhance its compatibility with POCT.

In this work, we developed the RPA-SCAN glass nanopore electronic sensing method for highly specific and sensitive MPXV detection. Our developed RPA assay rapidly completed pre-amplification in 20 minutes, and the SCAN sensor precisely detected cleaved single-stranded DNA (ssDNA) reporters via CRISPR, unaffected by RPA reagents or CRISPR proteins. We evaluated ssDNA cleavage over time, determined the limit of detection (LoD) for both RPA assay and SCAN sensor, and categorized samples using specific event rates and interarrival time thresholds. The specificity of the SCAN device was also tested against the Cowpox virus. Integrating the RPA-CRISPR with the nanopore sensor will open a new area for POCT applications.

2. Results and discussion

2.1 Working principle

Fig. 1 outlines the workflow of an RPA-SCAN device for MPXV detection, involving four main steps: sample collection, viral dsDNA amplification via RPA, ssDNA reporter cleavage by active Cas12 assay, and ssDNA reporter measurement with a nanopore sensor. The top panel illustrates sample collection, RPA, and CRISPR principles, while the bottom panel demonstrates how the nanopore sensor distinguishes between positive and negative samples.

To enhance the sensitivity and specificity of the overall SCAN sensor, we used the RPA-CRISPR reaction system. Fig. 1(a) illustrates the procedure: lesion swabbing, transport to a virus-

specific medium, isothermal nucleic acid amplification using RPA at 37°C (Q. Chen et al., 2023), and ssDNA reporter cleavage via Cas12 (Kim et al., 2021). RPA offers rapid reaction without the need for thermal or chemical melting. It uses lyophilized reagents, including recombinase protein, single-stranded DNA binding (SSB) protein, DNA polymerase protein, and MgOAc (Mg²⁺), which remain stable at room temperature, eliminating storage concerns. After 20 min of RPA, amplicons are mixed with CRISPR RNAs (crRNA) and Cas12a, called Ribonucleoprotein (RNP). Cas12a interacts with specific complementary DNA (cDNA), activating trans-cleavage and generating fragmented ssDNAs. Without MPXV double-stranded DNA (dsDNA), RNP remains inactive, keeping the circular ssDNA reporter unchanged, as shown in Fig. S1(a). M13mp18 ssDNA (7.49 kbp) was chosen for its accessibility, high signal-to-noise ratio (SNR), and established success in nanopore experiments (Nouri et al., 2020).

The integration of RPA and CRISPR in nanopore sensor improves the sensitivity and specificity of the sensor. Fig. 1(b) illustrates the capability of the nanopore sensor to classify the positive or negative sample using ssDNA fragments. The current trace (I-t trace) diagram shows variations in ssDNA reporter length for positive samples and typically shorter current dip, while negative samples maintain a consistent length. We intentionally stopped the reaction at 25 min to measure the cleaved reporter within nanopore size resolution (Li et al., 2023), keeping SNR ≥ 5 and Root mean square (RMS) noise \leq 3.57. Positive and negative readings can also be differentiated through the interarrival time counts and event rates. A steeper slope in the left panel of Fig. 1(c) indicates enhanced cleavage of reporter fragments in positive samples due to the CRISPR reaction with mother, daughter, and granddaughter molecules. The right panel of Fig. 1(c) reveals more events in positive samples, setting a threshold event at 13 min⁻¹ based on μ +3 σ , where $\mu=10 \text{ min}^{-1}$ and $\sigma=1 \text{ min}^{-1}$ of negative samples. The distribution of dwell time-current blockage and event charge deficits (ECD) showed positive and negative differences. ECD is calculated by multiplying blockage current and dwell time (Soni et al., 2022). As shown in Fig. S1(b), there is a shift from longer dwell times associated with larger blockages to shorter durations paired with smaller blockages. In the ECD diagram, the event rate moved leftward due to the decreasing size of the mother reporter and increasing cleaved reporter and number of events, as shown in **Fig. S1(c)**.

To confirm that the readings from our nanopore sensors were only from the ssDNA reporter and not from other molecules, Fig. S2(a) was tested with an RNP (34 nM), RPA reagents, and an

amplified MPXV DNA sample, excluding the use of the ssDNA reporter. The nanopore sensor cannot detect DNA segments shorter than 200 base pairs (bp) due to its resolution limitations (Li et al., 2023); as a result, reporters cleaved below this threshold, RPA amplicons and proteins remain undetected. After 15 min into the experiment, the current trace looked like results from an earlier test (Nouri et al., 2021). Furthermore, in **Fig. S2(b)-(d)**, we inspected only the ssDNA reporter's current trace and event rate distribution by decreasing the applied bias from 0.1 to 0.4 mV, assessing the assay's linearity. An R²= 0.98 was achieved, demonstrating strong linearity (Nouri et al., 2020). **Fig. 1(d)** displays the gel image utilized to validate the overall assay of the SCAN device. This Figure shows a smeared band for the positive control (PC) samples. The notemplate control (NTC) band remains consistent, indicating no RPA amplification of viral dsDNA, with no cleavage of ssDNA in the CRISPR reaction. The proposed SCAN sensor accurately detects MPXV viral dsDNA and can differentiate between positive and negative cases via RPA amplification. This method offers a potential tool for early MPXV detection for POCT applications.

2.2 RPA-CRISPR assay development and validation

We validated the RPA-CRISPR assay to assess the sensitivity and quantification of the SCAN sensor in MPXV detection. This involved integrating the CRISPR-Cas12a system with RPA, targeting the F3L gene fragments of the 2022 USA MPXV strain, specifically the 46,337 bp to 46,453 bp region (Fig. 2(a)). Primer and crRNA design details are provided in Supplementary data Table S1.

We first developed an RPA assay to enhance the sensitivity of the assay and established LoD. In an RPA reaction (**Fig. 1(a)**), recombinases form complexes with primers to identify homologous sequences in dsDNA. An SSB protein stabilizes the D-loop, Mg²⁺ enhances structure and catalysis, and DNA polymerase amplifies DNA at 39°C. The recipe for the RPA reaction can be found in **Supplementary Section 1.2.** data **Table S2**. In **Fig. 2(b)**, After 20 min of RPA, successful amplification was verified using gel electrophoresis, showing intensified bands at 117 bp, with some weak bands due to cross-dimerization, especially at lower concentrations (Ivanov et al., 2021). In **Fig. 2(c)**, the LoD for our RPA assay was approximately 19 copies/μL of stock sample at 95% confidence using 1 μL target in a 50 μL reaction, based on positive result in seven experiments; see Supplementary data **Table S3**, similar to other Lod results (Q. Chen et al., 2023;

Mills et al., 2023). Further method details are discussed in Supplementary Sections 1.2 and 1.5.

The PCR experiments were carried out using the identical RPA primers set to validate the RPA assay. **Fig. S3(a)** shows the amplification curve of PCR results; details are provided in **Supplementary Section 1.3.** To evaluate the linearity of the PCR experiments, the C_t values were plotted against serially diluted concentrations, ranging from 10⁵ copies/μL down to 1 copy/μL. The resulting linearity is shown in **Fig. S3(b)**, with an R² value of 0.99. However, no amplification from the PCR was observed at less than 10 copies/μL. **Fig. S3(c)** shows that the LoD of the PCR was 16 copies/μL, which is closely aligned with the RPA LoD and validates the RPA assay.

For sequence-specific recognition of MPXV dsDNA, a unique crRNA was designed. 10 μ L of RPA-amplified positive samples were used to demonstrate the real-time CRISPR-Cas12a assay with the 10 μ L (2 μ M) Deoxyribonuclease Alert (DNaseAlert) probe in a 100 μ L reaction; see **Supplementary Section 1.4**. In **Fig. S4**, a custom-made 5X buffer was used (Supplementary data **Table S5**) for a faster reaction, ensuring most of the ssDNA reporters were cleaved within 25 min. In **Fig. 2(d)**, the experiments showed that RPA-amplified targets effectively participate in the CRIPSR reaction, activating the Cas12a. Linearity was confirmed by comparing relative fluorescence units (RFU) across all CRISPR-Cas12a assays in **Fig. 2(e)**, where the RFU was considered after 45 mins of CRISPR reaction. The assay demonstrated linearity, with an R² value of 0.98. Based on the results above, the RPA-CRISPR assay seems to be well-suited for the SCAN sensor.

2.3 Size distribution of ssDNA reporters Utilizing SCAN

The size distribution of the ssDNA reporters of the CRISPR-RPA assay was assessed to validate the results of the SCAN sensor. The amplified sample (10⁴ copies/μL) from the RPA reaction was used to conduct the CRISPR reaction from 0 to 25 min. The reaction was halted at intervals of 0, 2, 5, 8, 15, and 25 min. The CRISPR reaction was validated through gel electrophoresis, and the ssDNA reporters were detected using a glass nanopore with a 300 mV applied potential (**Fig. S5**).

First, gel electrophoresis was used to verify the cleavage activity of the Cas12a. In **Fig. 3(a)**, the primary reporters displayed a 2.5-3.5 kbp band. Secondary reporters appeared after 2 min, indicating fragmentation of the primary reporters. As the reaction time progressed, cleaved primary reporters increased. By 25 min, the primary ssDNA reporters were almost undetectable,

indicating continuous trans-cleavage effects on both mother and daughter reporters. The gel protocol is discussed in **Supplementary Section 1.5** in more detail.

To validate the gel result, a glass nanopore was used to assess the size counting of the reporter. In **Fig. S6(a)**, the current-voltage relationship (I-V) indicated a pore diameter of 9.5-10 nm (Lastra et al., 2022). The activity of the Cas12a enzyme was halted in the CRISPR reaction by adding 1M KCl. In **Fig. S6(b)**, the baseline for 1M KCl was measured to observe the stability of the signal. The details of nanopore fabrication, data analysis, and sensing are provided in **Supplementary Sections 1.6** and **1.7**. Nanopore single molecule counting initially analyzed the 500 pM ssDNA reporters. In **Fig. 3(b)**, we categorized events by ECD (0.07 pC bin size). The shift in ECD distribution from right to left as the reaction progressed was observed, with the uncleaved reporter remaining on the right side of the dotted line. **Fig. 3(c)** illustrates dwell time and ionic current blockage changes with reaction time. As time passes, there's a clear shift in current blockage and dwell time, leading to reduced event rates for larger ECDs (longer reporters) and increased rates for smaller ECDs (shorter reporters).

We conducted measurements of the normalized count of interarrival time and the event rate to differentiate between positive and negative calls. Fig. 3(d) demonstrates an exponential (Poisson) distribution for interarrival time data sets, fitted using $P(t) = \lambda e^{-\lambda t}$, with λ representing the expected single-molecule event rate (Nouri et al., 2019). A steeper slope and smaller molecules are observed as the reaction progresses. In Fig. 3(e), a minimum of 2 min CRISPR reaction time is required to obtain a positive result, validated by the 3rd lane of the gel image in Fig. 3(a). Lower concentrations of amplicons lead to slower reactions (Fig. 2(d)), but the nanopore sensor remains reliable for rapid signal detection. Consequently, the SCAN sensor can pick up signals from the cleavage of ssDNA reporters and differentiate positive and negative signals in a brief timeframe.

2.4 Analytical LoD of MPXV SCAN

The analytical sensitivity of the MPXV SCAN sensor was evaluated, providing a foundation for understanding its performance in detecting low concentrations of the target. We employed MPXV virus amplicons ranging from 10^4 to 1 copies/ μ L and used nuclease-free water as NTC. Three positive samples were selected for concentrations between 10^2 and 10^4 copies/ μ L, while all positive samples were used for concentrations from 1 to 10^2 copies/ μ L (31 samples in total). The experiment was stopped after a 25-min CRISPR reaction. **Fig. 4(a)** shows the current trace of the

positive samples, showing variations in event rate and current dip length over time. We observed that the reaction speed is slower for lower concentrations than for higher ones, as the number of events varies between high and low concentrations. The results are shown in **Fig. S7(a)** by looking at the event rates for one positive sample at every concentration and the negative samples. Meanwhile, **Fig. 4(b)** demonstrates the blockage current distribution, shifting from a focus to a broader distribution from left to right, and the ECD distribution in **Fig. 4(c)** indicates an increase in the number of uncleaved products moving from left to right, revealing the slow reaction rate for the low number of amplified samples in RPA reaction.

We presented the event rate distribution to differentiate between positive and negative outcomes. The summary of all 31 samples mentioned above is presented in **Fig. 4(d)**. A threshold $(\mu + 3\sigma)$ was set based on six negative control experiments, as visualized in **Fig. S7(a)**. Event counts recorded over a 10-min period were averaged, targeting a significant event count (> 100) to reduce the standard deviation of the outcome (Nouri et al., 2019). Positive and negative determinations were also compared using the normalized count inter-arrival duration (**Fig. S7(b)**). Using the Poisson distribution formula, $P(t) = \lambda e^{-\lambda t}$, a threshold slope was established where λ =13 events min⁻¹. Variations in the reaction rate were observed for samples with lower copy counts. It can be because the signal from one or two copies overlapped statistically, yet the results still indicate positive. Lastly, **Fig. 4(e)** outlines the SCAN sensor's LoD. We determined the overall LoD to be 16 copies/ μ L by classifying results as positive or negative with a 95% confidence level, which closely matches our RPA and PCR assay outcomes. However, the difference in LoD between RPA and SCAN sensors is due to the noise of the sensor. The above results show that the SCAN sensor can detect MPXV qualitatively.

2.5 Analytical Specificity Test of MPXV SCAN

We undertook specificity tests for the CRISPR reaction to ensure its precision in targeting only the desired genetic sequence, improving its specificity and accuracy. Genomic DNA from the Cowpox Brighton strain and MPXV virus (10⁴ copies/μL) was pre-amplified via RPA for 20 minutes. Then, 2 μL RPA amplicons were combined with 34 nM RNP and a reporter for Cas12a cleavage assays at 37°C, with reactions halted at 0 and 25 min for both Cowpox and MPXV virus. **Fig. 5(a)** shows the specificity analysis using 5 μM DNaseAlert reporters revealed significant RFU differences for MPXV, while Cowpox and NTCs had consistent signals. A threshold was

determined using the formula $\mu + 3\sigma$ (4890.208 A.U.), where μ =3467.289 A.U. and σ =474.306 A.U. denote the mean and standard deviation of R.F.U values for Cowpox and NTCs. This analysis confirmed a specificity of 100%. For further validation, **Fig. 5(b)** presents a gel electrophoresis result using a 10 nM ssDNA reporter. Notably, the ssDNA reporter remained intact for Cowpox, 0 min-MPXV, and NTC, while it was absent for 25 min-MPXV. A faint smeared band on the gel further shows the validity of reaction.

To validate specificity using the nanopore SCAN method, we employed a 500 pM ssDNA reporter (**Fig. 5(c)**). In current trace, Cowpox and 0 min-MPXV exhibited consistent event rates, while 25 min-MPXV showed an increased event rate. Positive and negative events were distinguished using a threshold (13 min-1) established as $\mu + 3\sigma$ (**Fig. 5(d)**). T-tests were conducted for Cowpox signals at 0 and 25 min, resulting in a *p*-value of 0.29, indicating no significant difference. However, for MPXV signals at 0 and 25 min, a *p*-value of 10^{-15} rejects the null hypothesis, highlighting the SCAN sensor's specificity for MPXV detection.

3. Conclusions

This work presents RPA-SCAN, a highly sensitive MPXV detection method combining Solid-state CRISPR-Cas12a Assisted nanopore with isothermal RPA. This method provides a sensitivity that unamplified SCAN cannot achieve while also addressing the challenges of PCR-SCAN for POCT applications. We demonstrated that size-counting of single molecules does not interfere with the reporter of CRISPR reaction, and it enables analysis of the reaction-time-dependent distribution of the cleaved reporter. We designed and validated the MPXV-specific RPA assay and achieved a LoD of 19 copies in a 50 µL reaction system. Utilizing the SCAN platform, the whole process could be completed within 55 min (20 min RPA, 25 min CRISPR assay, and 10 min nanopore analysis. We achieved the overall LoD of the SCAN sensor, which is 16 copies/µL (26.56 aM) of MPXV dsDNA at a 95% confidence level. We also verified the specificity of RPA-SCAN in distinguishing MPXV from cowpox virus with 100% accuracy. These results suggest that the isothermal RPA-SCAN is a promising tool for Monkeypox detection. In future work, we aim to address clinical applications and the lyophilization of reagents for field deployability. Given its electronic nature and miniaturization potential, the RPA-SCAN system paves the way for diagnosing various other infectious pathogens at the point of care.

4. Materials and methods

Materials and methods are described in the Supplementary Information.

Supplementary data

The Supplementary data to this article can be found online.

CRediT authorship contribution statement

Md. Ahasan Ahamed: Conceptualization, Methodology, Formal analysis, Investigation, Visualization, Writing – original draft, Writing – review & editing. Muhammad Asad Ullah Khalid: Methodology, Validation, Writing – review & editing. Ming Dong: Methodology, Software, Resources. Anthony J. Politza: Software, Resources. Zhikun Zhang: Validation, Resources. Aneesh Kshirsagar & Tianyi Liu: Writing – review & editing. Weihua Guan: Conceptualization, Supervision, Writing – review & editing, Resources, Funding acquisition.

Acknowledgments

This work was partially supported by the National Institutes of Health (R33AI147419) and the National Science Foundation (1902503, 1912410, 2045169). Any opinions, findings, conclusions, or recommendations expressed in this work are those of the authors and do not necessarily reflect the views of the National Science Foundation and National Institutes of Health.

Declaration of competing interest

The authors declare no conflict of interest.

Data Availability Statement

Data will be made available on request.

Figures and Captions

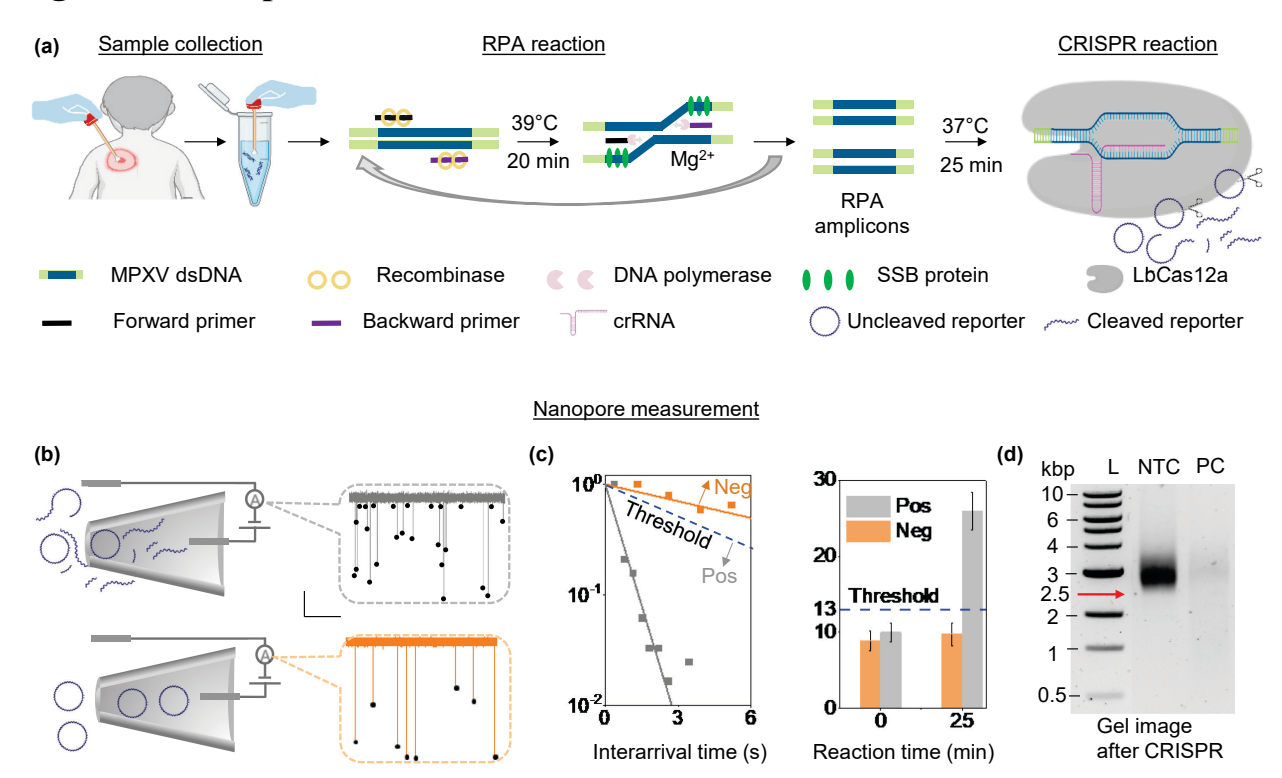


Fig. 1. RPA-SCAN Sensor Workflow for MPXV Detection. a) Collection and preparation of swab samples, followed by RPA amplification at 39°C for 20 minutes. Activation of the CRISPR reaction leads to circular ssDNA reporter cleavage. b) Nanopore readout, Cleaved reporters in positive samples appear as daughter and granddaughter reporters, causing a significant event rate increase. Negative samples show the ssDNA reporter as the mother reporter, causing a negligible event rate. This differentiation enables classification based on the current trace. c) Positive or negative call. A steeper slope in the normalized interarrival counts plot indicates positive samples with more cleaved reporter fragments, while a less steep slope signifies no cleavage. Positive samples exhibit a higher event rate in the Event Rate plot, with a threshold of 13 min⁻¹ for positive designation. d) Validation of SCAN result by Gel Electrophoresis. Positive control (PC) shows cleaved reporters with a smeared band, while the no template control (NTC) maintains a consistent reporter at the 2.5 kbp position.

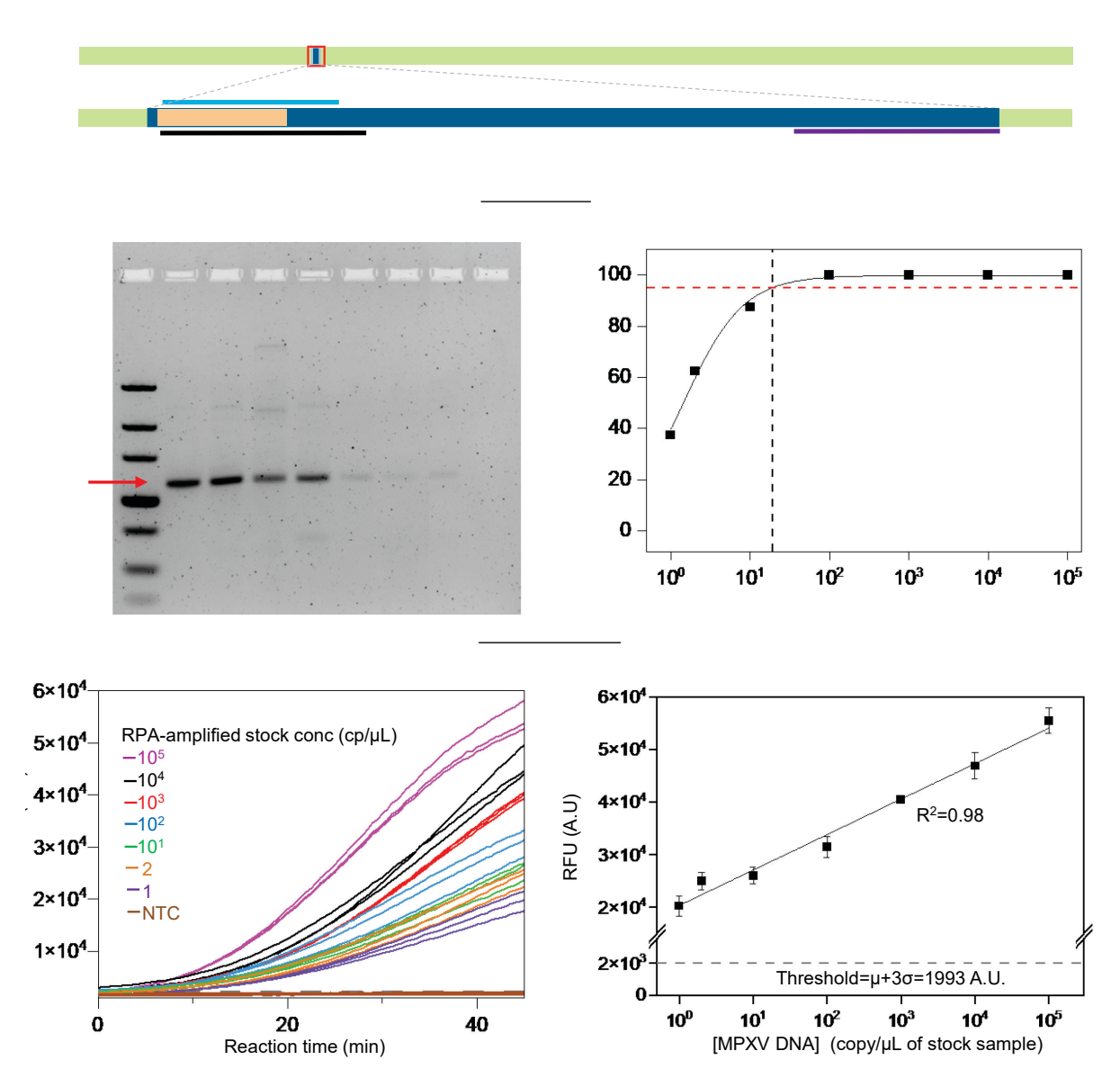


Fig. 2. RPA-CRISPR assay design and validation. a) The F3L gene of MPXV served as the target region for RPA and CRISPR reactions using forward (F) and reverse (R) primers. b) Gel electrophoresis image displaying RPA reactions on serially diluted MPXV dsDNA (10^5 copies/μL to 1 copy/μL). c) The LoD of the RPA assay was found to be 19 copies in a 50 μL reaction volume using 1 μL of the target. (P=positive, T=total reactions, n=8). d) Real-time CRISPR results using DNaseAlert and analyzing three positive reactions from **Fig. (c)**. e) The linearity is demonstrated by plotting the endpoint RFU after 45 min; the threshold was calculated based on mean (μ) and standard deviation (σ) of NTCs. An R² value of 0.98 indicates a strong correlation.

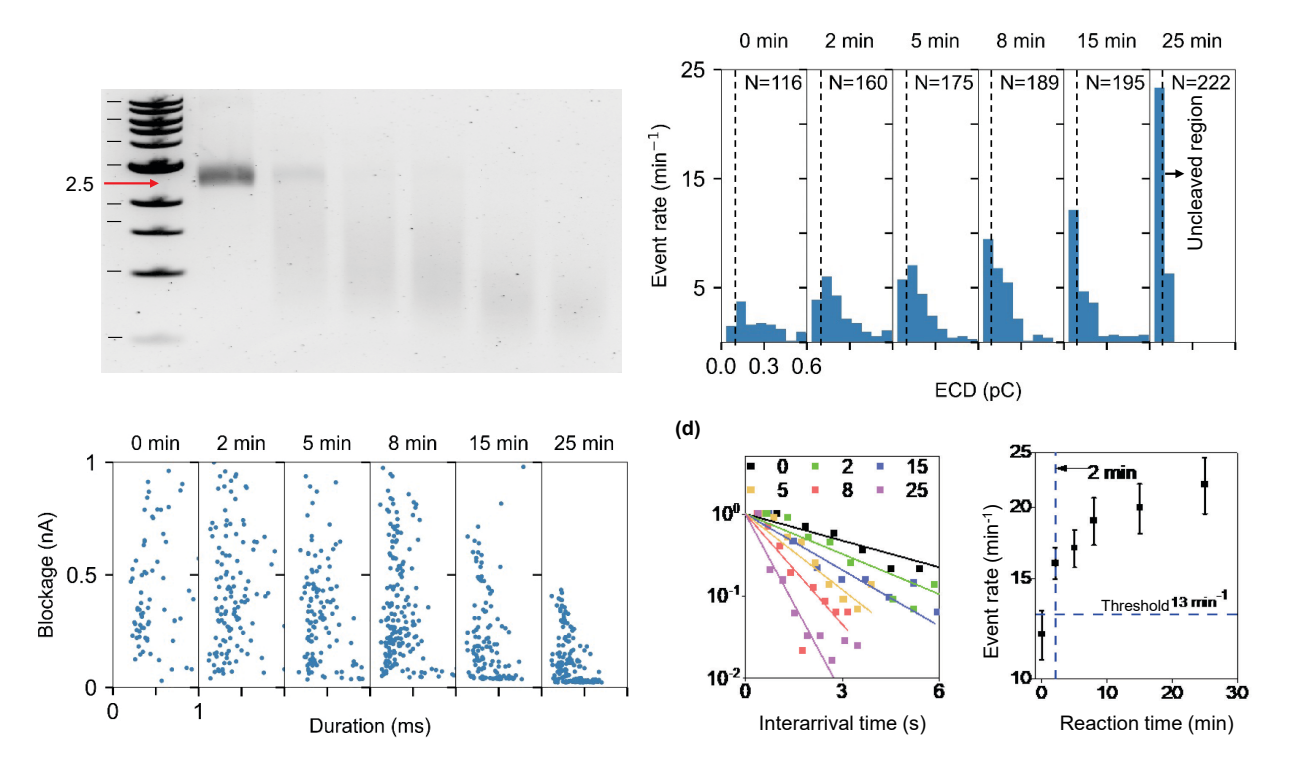


Fig. 3. Size distribution of ssDNA reporter using SCAN (a) Gel electrophoresis data at reaction halting times from 0 to 25 min, with 34 nM RNP and 10 nM reporter concentrations. (b) Event rate distribution at ECD values 0.07 to 0.6 Pico-coulomb (pC). The region right of the dashed line is the no cleavage zone. N represents the total event counts for each reaction time. (c) Blockage current and dwell times distribution for ssDNA reporter at various reaction intervals. (d) Normalized counts of interarrival time at different CRISPR reaction stopping times. The straight line depicts exponential fits, with a steeper slope indicating faster cleavage. (e) The event rate increased significantly from 0 min to 25 min. The vertical dashed line shows the nanopore's ability to distinguish positive and negative samples within 2 minutes at 10⁴ copies/ μL. Measurements were at the 10-minute mark with a 1 M KCl salt concentration and 0.3 V applied bias.

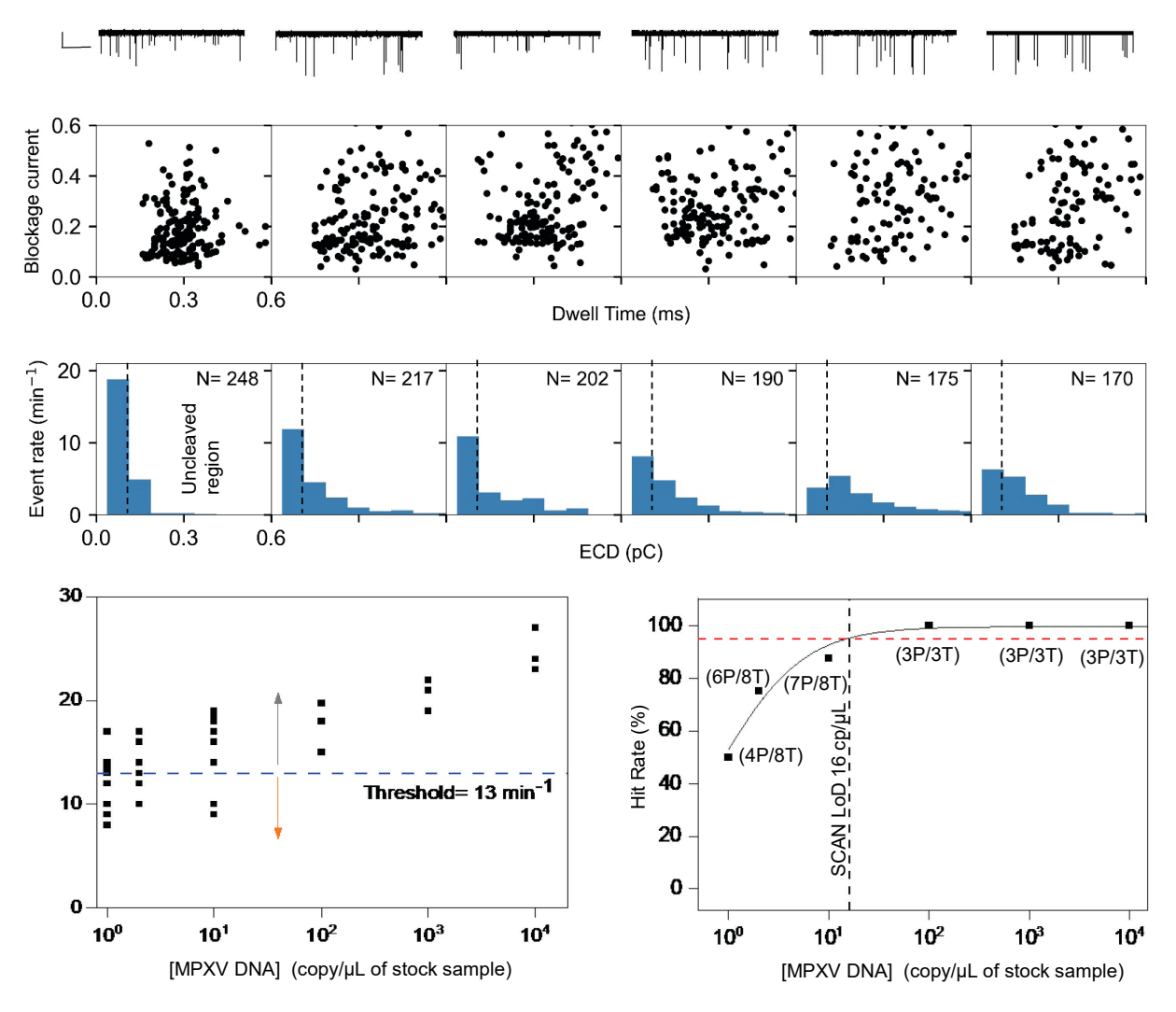


Fig. 4. Analytical Limit of Detection(LoD) of MPXV SCAN a) Current trace of positive samples at different concentrations on serially diluted MPXV dsDNA (10^4 copies/ μ L down to 1 copy/ μ L), indicating shifts in event rate and current dip length. b) Distribution of blockage current, transitioning from a focus to a broader region. c) ECD distribution, showing a left-to-right progression of uncleaved products. d) Summary of all 31 tested samples, including a threshold derived from six negative control experiments. e) Determination of the SCAN sensor's overall LoD set at 16 copies/ μ L based on a 95% confidence interval.

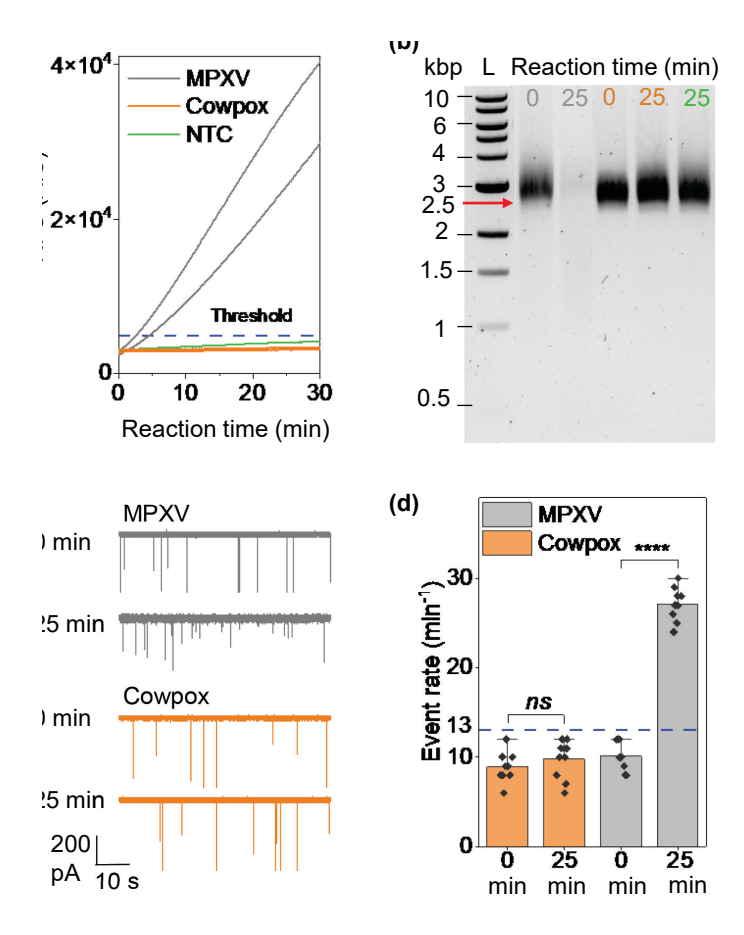


Fig. 5. Evaluation of MPXV SCAN's Analytical Specificity. a) Assessment of MPXV virus specificity using RFU at a concentration of 10^4 copies/μL employing DNaseAlert probe. The Cowpox virus and the NTCs demonstrated stable RFU values, unlike MPXV. Achieving 100% specificity used a threshold of $\mu + 3\sigma$ (4890.208 A.U.). b) Gel electrophoresis validation, illustrating the differential responses of the 10 nM ssDNA reporters for Cowpox and MPXV. c) SCAN confirmation, depicting current traces at 0- and 25-min post-reaction. Consistent event rates appeared for Cowpox and the 0-min MPXV sample, while a remarkable event rate was observed for the 25-min MPXV sample. d) Differentiating between positive and negative detections using a threshold set at 13 min⁻¹, as the dashed line shows. p>0.05 fails to reject the null hypothesis, suggesting no significant (ns) difference in the signals' means and medians. Conversely, $p=10^{-15}$ highlighted substantial differences, emphasizing SCAN sensor accuracy.

Reference

Ahamed, Md.A., Reza, M.I., Al-Amin, Md., 2020. J. Adv. Eng. Comput. 4(2), 140-148.

Ahamed, Md.A., Kim, G., Li, Z., Kim, S.-J., 2022. Anal. Chim. Acta 1236, 340587.

Ali, M., Khalid, M.A.U., Kim, Y.S., Soomro, A.M., Hussain, S., Doh, Y.H., Choi, K.H., 2021. J. Electrochem. Soc. 168, 037507.

Americo, J.L., Earl, P.L., Moss, B., 2023. Proc. Natl. Acad. Sci. 120, e2220415120.

Chadha, J., Khullar, L., Gulati, P., Chhibber, S., Harjai, K., 2022. Environ. Microbiol. 24, 4547–4560.

Chen, J.S., Ma, E., Harrington, L.B., Da Costa, M., Tian, X., Palefsky, J.M., Doudna, J.A., 2018. Science 360, 436–439.

Chen, Q., Gul, I., Liu, C., Lei, Z., Li, X., Raheem, M.A., He, Q., Haihui, Z., Leeansyah, E., Zhang, C.Y., Pandey, V., Du, K., Qin, P., 2023. J. Med. Virol. 95.

Dey, P., Bradley, T.M., Boymelgreen, A., 2023. Sci. Rep. 13, 6370.

Di Giulio, D.B., Eckburg, P.B., 2004. Lancet Infect. Dis. 4, 15–25.

Elsayed, S., Bondy, L., Hanage, W.P., 2022. Clin. Microbiol. Rev. 35, e00092-22.

Farooqi, H.M.U., Kang, B., Khalid, M.A.U., Salih, A.R.C., Hyun, K., Park, S.H., Huh, D., Choi, K.H., 2021. Nano Converg. 8, 3.

Ivanov, A.V., Safenkova, I.V., Zherdev, A.V., Dzantiev, B.B., 2021. Anal. Chem. 93, 13641–13650.

Kellner, M.J., Koob, J.G., Gootenberg, J.S., Abudayyeh, O.O., Zhang, F., 2019. Nat. Protoc. 14, 2986–3012.

Khalid, M.A.U., Kim, K.H., Chethikkattuveli Salih, A.R., Hyun, K., Park, S.H., Kang, B., Soomro, A.M., Ali, M., Jun, Y., Huh, D., Cho, H., Choi, K.H., 2022. Lab. Chip 22, 1764–1778.

Kidan, L., Kyeong-Beom, P., Hyung-Jun, K., Jae-Seok, Y., Hongsik, C., Hyun-Mi, K., Ki-Bum, K., 2018. Adv Mater 30, 1704680(1–28).

Kim, H., Lee, S., Yoon, J., Song, J., Park, H.G., 2021. Biosens. Bioelectron. 194, 113587.

Lastra, L.S., Bandara, Y.M.N.D.Y., Nguyen, M., Farajpour, N., Freedman, K.J., 2022. Nat. Commun. 13, 2186.

Lau, H.Y., Wang, Y., Wee, E.J.H., Botella, J.R., Trau, M., 2016. Anal. Chem. 88, 8074–8081.

Li, H., Li, Y., Gui, C., Chen, D., Chen, L., Luo, L., Huang, G., Yuan, Y., He, R., Xia, F., Wang, J., 2023. Talanta 256, 124275.

Li, S.Y., Cheng, Q.X., Liu, J.K., Nie, X.Q., Zhao, G.P., Wang, J., 2018. Cell Res 28, 491–493.

Lillis, L., Siverson, J., Lee, A., Cantera, J., Parker, M., Piepenburg, O., Lehman, D.A., Boyle, D.S., 2016. Mol Cell Probes 30, 74–8.

Lobato, I.M., O'Sullivan, C.K., 2018. Trends Anal. Chem 98, 19–35.

Mills, M.G., Juergens, K.B., Gov, J.P., McCormick, C.J., Sampoleo, R., Kachikis, A., Amory, J.K., Fang, F.C., Pérez-Osorio, A.C., Lieberman, N.A.P., Greninger, A.L., 2023. J. Clin. Virol. 159, 105373.

Notomi, T., Mori, Y., Tomita, N., Kanda, H., 2015. J. Microbiol. 53, 1–5.

Nouri, R., Jiang, Y., Lian, X.L., Guan, W., 2020. ACS Sens 5, 1273-1280.

Nouri, R., Jiang, Y.Q., Tang, Z.F., Lian, X.L., Guan, W.H., 2021. Nano Lett 21, 8393-8400.

Nouri, R., Tang, Z.F., Guan, W.H., 2019. Anal Chem 91, 11178–11184.

Okyay, R.A., 2022. Eurasian J. Med. Oncol.

Petralia, S., Conoci, S., 2017. ACS Sens. 2, 876–891.

Qin, P., Park, M., Alfson, K.J., Tamhankar, M., Carrion, R., Patterson, J.L., Griffiths, A., He, Q., Yildiz, A., Mathies, R., 2019. ACS Sens 4, 1048–1054.

Sakata, T., Kamahori, M., Miyahara, Y., 2005. Jpn. J. Appl. Phys. 44, 2854.

Sharma, A., Priyanka, Fahrni, M.L., Choudhary, O.P., 2022. Int. J. Surg. 104, 106812.

Soni, N., Freundlich, N., Ohayon, S., Huttner, D., Meller, A., 2022. ACS Nano.

Wang, Z., Liu, Y., Yu, L., Li, Y., Qian, G., Chang, S., 2019. Analyst 144, 5037–5047.

Graphical abstract

